Structural and biochemical mechanism for increased infectivity and immune evasion of Omicron BA.1 and BA.2 variants and their mouse origins

Youwei Xu[1,8], Canrong Wu[1,8], Xiaodan Cao[2,8], Chunyin Gu[2,8], Heng Liu[1,8], Mengting Jiang[3,1], Xiaoxi Wang[1], Qingning Yuan[1,4], Kai Wu[1,4], Jia Liu[2], Xianqing He[2], Deyi Wang[2], Xueping Wang[2], Su-Jun Deng[2]✉, H. Eric Xu[1,5,6]✉, Wanchao Yin[1,5,7]✉

[1] The CAS Key Laboratory of Receptor Research, Shanghai Institute of Materia Medica, Chinese Academy of Sciences, Shanghai 201203, China

[2] Shanghai Jemincare Pharmaceuticals Co., Ltd., Shanghai 201203, China

[3] School of Chinese Materia Medica, Nanjing University of Chinese Medicine, Nanjing 210023, China

[4] The Shanghai Advanced Electron Microscope Center, Shanghai Institute of Materia Medica, Chinese Academy of Sciences, Shanghai 201203, China

[5] University of Chinese Academy of Sciences, Beijing 100049, China

[6] School of Life Science and Technology, ShanghaiTech University, Shanghai 201210, China

[7]Zhongshan Institute for Drug Discovery, Shanghai Institute of Materia Medica, Chinese Academy of Sciences, Guangdong 528400, China

[8]These authors contributed equally: Youwei Xu, Canrong Wu, Xiaodan Cao, Chunyin Gu, Heng Liu

✉ Correspondence should be addressed to Su-Jun Deng (dengsujun@jemincare.com) or H. Eric Xu (eric.xu@simm.ac.cn) or Wanchao Yin (wcyin@simm.ac.cn)

ABSTRACT

The Omicron BA.2 variant has become a dominant infective strain worldwide. Receptor binding studies reveal that the BA.2 spike trimer have 11-fold and 2-fold higher potency to human ACE2 than the spike trimer from the wildtype and Omicron BA.1 strains. The structure of the BA.2 spike timer reveals that all three receptor-binding domains (RBD) in the spike trimer are in open conformation, ready for high affinity binding to human ACE2, providing the basis for the increased infectivity of the BA.2 strain. JMB2002, a therapeutic antibody that was shown to have efficient inhibition of Omicron BA.1, also shows potent neutralization activities against Omicron BA.2. In addition, both BA.1 and BA.2 spike trimers are able to bind to the mouse ACE2 with high potency. In contrast, the wildtype spike trimer binds well to cat ACE2 but not to mouse ACE2. The structures of both BA.1 and BA.2 spike trimer bound to mouse ACE2 reveal the basis for their high affinity interactions. Together, these results suggest a possible evolution pathway for Omicron BA.1 and BA.2 variants from human-cat-mouse-human circle, which could have important implications in establishing an effective strategy in combating viral infection.

INTRODUCTION

The Omicron variants BA.1 and BA.2 of severe acute respiratory syndrome coronavirus 2 (SARS-CoV-2), the causative virus of COVID-19, are two sister variants of concerns (VOCs) that have infected hundreds of millions of people worldwide.[1] In particular, the BA.2 strain has overtaken the BA.1 strain to become the current dominant infective strain that continues to rampage across the globe (Fig. 1a).[2] Both BA.1 and BA.2 strains are evolved independently from predominant VOC strains, including Alpha, Beta, Gamma, and Delta variants.[3] Mutational profile analysis suggests that the Omicron variants may arise from evolution through mouse as a host.[4] The biochemical and structural basis for the viral infection to mouse remains largely unknown.

The trimeric spike protein is a major membrane surface glycoprotein of SARS-CoV-2 that mediates the binding to the host receptor ACE2 and subsequent viral entry into cells.[5-7] The matured spike protein contains two subunits: an ACE2 binding S1 subunit and a membrane-fusion S2 subunit. Within the S1 subunit is an N-terminal domain (NTD) of unknown function and a C-terminal receptor-binding domain (RBD). The S2 subunit contains a conserved fusion peptide (FP) motif that is mostly hydrophobic and capable of mediating viral fusion with host cells[7]. Extensive structures of the spike trimer reveal the open and closed conformations for the three RBD within the spike trimer, where the open “up” RBD conformation is prerequisite for ACE2 binding.[6, 8-11] Upon ACE2 binding, the spike trimer undergoes conformational changes to expose the FP motif of the S2 subunit to initial membrane fusion that allow viral entry into the host cells.[12]

The spike protein is also the major target of immune response during infection and therapeutic antibodies.[13-17] Most VOCs such as the Delta variant contain 7-10 mutations in the spike protein. In contrast, Omicron BA.1 and BA.2 have 37 and 31 mutations in their spike proteins, respectively.[18] Structural studies of the Omicron BA.1 spike trimer reveal that most of the 37 mutations are mapped on the surface of the spike protein, with many of them enriched in known epitopes of therapeutic antibodies.[3, 19, 20] In addition, the Omicron BA.1 spike protein binds to the human ACE2 with 6-7 fold higher potency and the Omicron spike trimer is less stable and prone to the open “up” conformation that is ready to interact with ACE2[3]. These studies have provided the molecular basis for the increased infectivity and immune evasion of Omicron BA.1 to vaccine and therapeutic

antibodies. However, the Omicron BA.2 variant has even more capacity in viral transmission and has surpassed BA.1 as the dominant infective strain currently in many regions across the world (Fig. 1a).[2] The Omicron BA.2 spike protein has 11 amino acid difference in 8 locations from the BA.1 spike protein (Supplementary information, Fig. S1), more than 7 amino acid difference of the Delta variant from the original wild type strain.

Although the symptoms of infection by Omicron BA.1 and BA.2 appear to be less severe,[21] antibody therapy may be essential for critically ill patients. JMB2002, a broad-spectrum therapeutic antibody, is known to inhibit both the wildtype strain and the Omicron BA.1 variant.[3, 22] However, the efficacy of JMB2002 against the Omicron BA.2 is unknown. In this paper, we report the cryo-EM structures of the Omicron BA.2 spike trimer in complex with the human ACE2 and JMB2002. We also determined the spike trimer from both BA.1 and BA.2 in complex with the mouse ACE2. Together with comprehensive biochemical studies, our structures provide a basis for the higher transmission and immune evasion of the Omicron BA.2 variant and possible mouse origins of Omicron BA.1 and BA.2 variants.

RESULTS

Characterization of the interaction of the Omicron BA.2 spike trimer with hACE2

To study the mechanism for enhanced transmission of Omicron BA.2, we first characterized the interaction between the human ACE2 (hACE2) with the spike extracellular domain trimer from SARS-CoV-2 Omicron BA.2, BA.1, and wildtype (WT) strains, all of which contain the protein engineering mutations on furin cleavage site and proline substitutions (2P or 6P) to stabilize the prefusion conformation. Dimeric hACE2 bound to immobilized Omicron BA.2 spike trimer with a dissociation constant (K_D) value of 0.4 ± 0.1 nM, which is approximately 11-fold higher than that with WT spike trimer (K_D =4.7 ± 0.6 nM) and is nearly 2-fold higher than that with BA.1 spike trimer (K_D =0.75 ± 0.1 nM). (Fig.1b and 1c). We also examined the interactions of monomeric hACE2 with Omicron BA.2 spike trimer with the K_D value of 3.2 ± 0.7 nM, which is approximately 5-fold higher than that with WT spike trimer (K_D =15.0 ± 0.6 nM) and is around 2-fold higher affinity than that with BA.1 spike trimer (K_D =6.4 ± 1.0 nM) (Supplementary information, Fig. S2). The observed interactions between hACE2 with WT spike trimer and between hACE2 with BA.1 spike trimer were consistent with previously published

data.[3] However, the enhanced interaction of Omicron BA.2 spike trimer protein with hACE2 maybe one of the key factors giving rise to its increased transmissibility and its power of overtaking Omicron BA.1 in a short period of time.

To gain structural insights into the higher affinity of the Omicron BA.2 spike trimer to hACE2, we reconstituted the Omicron BA.2 spike trimer-hACE2 complex by incubating Omicron spike trimer with an excess of hACE2, followed by size exclusion chromatography and the assembled sample was subjected to cryo-electron microscopy (cryo-EM) analysis (Supplementary information, Fig. S3). We observed two distinct structure states of the BA.2 spike trimer-hACE2 complex (Figs. 1d and 1e). In the first structure state, each spike molecule from Omicron BA.2 spike trimer binds to one hACE2 molecule and all three RBDs are in an open up position for hACE2 binding. Two RBD-hACE2s are with strong density, while the third one is less visible, suggesting partial occupancy of the third RBD under our experimental conditions (Fig. 1d). In the second structure state, two of three RBDs are in the open up position, both of which bind to hACE2. The density of the third RBD is in a clear down position and shows the direct interaction with an up RBD, which could stabilize one of the “up” RBDs, as it was observed previously (Fig. 1e).[3] Particle classification reveals that about 42% and 58% spike particles bind with hACE2 in 3:3 and 3:2 molar ratio, respectively, albeit an excess of hACE2 were incubated with spike trimer during the sample preparation. Notably, only one hACE2 bound to one RBD from the spike trimer was observed in our previous cryo-EM structural analysis of Omicron BA.1 spike trimer-hACE2 complex[3]. In contrast, in the Omicron BA.2 spike trimer-hACE2 complex, the spike trimer bound to at least two or three hACE2, indicating a more hACE2 binding tendency of the BA.2 spike trimer.

Mapping the 26 mutations onto the Omicron BA.2 spike trimer reveals that 23 mutations are distributed on the surface and 3 are on the interior of the spike trimer (Fig. 1f). Only 6 out of 26 mutations are different from BA.1, while the rest of the mutations share the same substitutes with BA.1. Similar with 15 mutations in RBD of BA.1 spike, 16 mutations are located on the RBD domain of BA.2 spike (Fig. 1g), which serves as ACE2 binding and the epitopes for 90% of antibodies[3, 23-25]. These mutations could cause the immune evasion to vaccines and therapeutic antibodies[26], however, some antibodies which do not rely on those sites could retain the immunity.

Focus refinement on RBD-hACE2 region resulted a reconstruction map at 3.0 Å resolution (Supplementary information, Fig. S4). The cryo-EM density map was of sufficient quality to enable us to build an atomic model of the RBD-hACE2 structure (Fig. 2a). The overall assembly of the Omicron BA.2 RBD-hACE2 complex closely resembles Omicron BA.1 RBD-hACE2 complex, where the receptor binding motif (RBM) is identical. Briefly, the side chain of Q493R forms a new salt bridge with E35 on hACE2, Q498R forms a new salt bridge with D38 of hACE2, and K417N losses a salt bridge (Figs. 2b and 2c), these key mutations resulted in an enhanced binding to hACE2, although the sum of other mutations lead to the loss of few hydrogen-bonded interactions. Thermal shift assays showed that the spike trimers from Omicron BA.2, Omicron BA.1, and WT display two melting temperatures, which were assigned previously, with the lower Tm for the RBD and the higher Tm for the spike trimer.[3] The Tm values for the RBD from Omicron BA.2, Omicron BA.1, and WT are 47.4 °C, 44.5 °C, and 52.5 °C (Fig. 2d), respectively, indicating that RBD in Omicron BA.2 is a bit more stable than that from BA.1, but less stable than the WT. In the BA.2 RBD, the substitute of D405, N405 forms two inter-molecular hydrogen-bonds with the side chain of R403 and the main chain of G504 (Fig. 2e). The BA.1 RBD lacks these interactions because the distance between the side chain of D405 and R403 is about 4.5 Å (Fig. 2e). The additional interactions in the BA.2 RBD above could contribute to its higher stability than the BA.1 RBD. The lower Tm2, which corresponds to the dissociation of the BA.2 spike trimer, indicates its more dynamic than BA.1 spike trimer (Fig. 2d). Comparing the mutations on the S1 and S2 domains, three amino acids are different, including T547K, D856K, and L981F mutations on BA.1 strain but not in the BA.2 spike. Strikingly, D856K from protomer 1 forms a salt bridge with D571 from the other protomer, which could stabilize the BA.1 spike trimer (Fig. 2e). In BA.2 strain, D856 lacks such interaction, thus, the BA.2 spike trimer shows lower melting temperature under our thermal shift assays.

Inhibition of ACE2 binding to the BA.2 spike trimer by an anti-Omicron antibody JMB2002

Previously, we reported the potent neutralization activity of a clinical stage antibody, JMB2002, which could effectively neutralize Omicron BA.1 as well as variants Alpha, Beta, and Gamma, but not Delta.[3, 22] To evaluate the neutralizing activity of JMB2002 against the Omicron BA.2 variant, we first evaluated the binding of JMB2002 to the Omicron BA.2 spike trimer. JMB2002 Fab recognized the Omicron BA.2 spike trimer

with K_D of approximately 2.6 nM. Meanwhile, JMB2002 IgG bound to the Omicron BA.2 spike trimer with K_D of approximately 0.3 nM (Fig. 3a). Encouragingly, the JMB2002 Fab and IgG bound the Omicron BA.2 spike trimer with equal affinity compared with the Omicron BA.1 spike trimer, despite about 22 mutations different from BA.2 to BA.1 spike. As we would expect, JMB2002 effectively blocked the entry of the Omicron BA.2 pseudovirus into human ACE2-expressing cells in a pseudovirus neutralization assay, with the half-maximal inhibition concentration (IC_{50}) as 0.2 μg/ml (Fig. 3b), which is the same as for the inhibition of Omicron BA.1 pseudovirus. Taking together, JMB2002 is a broad-spectrum anti-SARS-CoV-2 antibody that has equal inhibition efficacy to both Omicron BA.1 and BA.2 strains.

To explore the basis of JMB2002 inhibition of Omicron BA.2, we solved the structure of the Omicron BA.2 spike trimer bound to a Fab from JMB2002 at a global resolution of 3.27 Å (Fig. 3c, and Supplementary information, Fig. S5), with the aid of the same nanobody to stabilize the constant regions of Fab as we used in the Omicron BA.1 study.[3] The cryo-EM density map reveals the binding of three Fab molecules, with each RBD (two up RBDs and one down) bound to one Fab (Figs. 3c and 3d), which was also similar to one of our previously solved structures of JMB2002 Fab bound to the Omicron BA.1 spike trimer.[3] The overall structure of the Omicron BA.2 spike trimer in the Fab-bound complex is very similar to that of the ACE2-bound complex, with a root mean square difference of 1.48 Å over all C_α atoms of the spike trimer, including the configuration of two up RBDs and one down. Superposition of the structures of hACE2-bound and Fab-bound Omicron BA.2 spike trimer, demonstrated that Fab-1 binding to the down RBD-1 would clash with hACE2-1 and hACE2-2, while Fab-3 binding to the up RBD-3 would clash with hACE2-3 (Fig. 3e). Thus, the binding of three Fabs to the spike trimer would completely block ACE2 binding.

Cross species binding of ACE2 with the Omicron spike trimer

In order to provide clues for mitigating current pandemic continuously causing global public health concern, we set up to investigate the potential evolution roadmap of Omicron variants. Firstly, we evaluated the cross-species ACE2 binding to the spike trimer of WT and Omicron BA.1 and BA.2 strains. Unlike human ACE2, which showed enhanced binding to the Omicron spike trimer, ACE2 from horse, pig, and sheep displayed decreased binding, with cat ACE2 protein showing similar binding between

WT and Omicron variants (Supplementary information, Fig. S2). Meanwhile, both the rat and dog ACE2 proteins showed no binding with WT, Omicron BA.1, or Omicron BA.2 trimer. To our surprise, we found that mouse ACE2 bound to both Omicron BA.1 and BA.2 spike trimer with high affinity (Figs. 4a and 4b), compared with no binding of mouse ACE2 to WT spike trimer (Fig. 4c). Moreover, the mouse ACE2 bound the Omicron BA.2 spike trimer with approximately threefold increased affinity (K_D = 2.9 ± 0.2 nM) compared with the Omicron BA.1 spike trimer (K_D = 9.1 ± 7.1 nM) (Figs. 4a, 4b and 4d).

Multiple sequence alignment of the key residues that are responsible for the interaction with SARS-CoV-2 spike trimer from representative species (human, mouse, cat, rat, and dog) reveals that 7 residues are highly conserved including S19, F28, E35, Y41, Q42, L45, and D355 (Fig. 4e and Supplementary information, Fig. S2). However, the rest 9 residues are partially replaced in different species comparing with human, thus led to a diverse binding behavior to SARS-CoV-2 spike trimer. A modelled BA.2 RBD-cat ACE2 structure based on the solved BA.2 RBD in this work and cat ACE2 structure derived from PDB entry 7C8D was superposed onto WT RBD-cat ACE2 structure (Fig. 4f),[27] which revealed that equal amount of hydrogen bonds in RBD-binding interface resulting a comparable binding capacity. Due to the sequence conservation of ACE2, we generated dog ACE2 and rat ACE2 by site mutations with the minimal clashes. The substituted residues lost polar interactions to BA.2 RBD, leading to the none or low binding affinity between dog ACE2 or rat ACE2 and BA.2 RBD, which is consistence with our binding data (Figs. 4g and 4h). In aggregate, our results show the determinant residues of ACE2 for cross-species specificity.

Cryo-EM Structures of BA.2 and BA.1 Spike binding with mACE2

To reveal the molecular basis for the high affinity binding of the Omicron BA.2 and BA.1 spike trimer to mouse ACE2, we determined their complex structures (Figs. 5a-5d, Supplementary information, Figs. S6 and S7). Two major states were observed for both BA.2-mACE2 and BA.1-mACE2 complexes, in which the spike trimer binds to one or to two mACE2. In the first state, one RBD is in the open up position with mACE2 binding, and the other two RBDs are in the close down conformation without mACE2 binding (Figs. 5a and 5c). The second state is with two RBDs in the open up position with mACE2 binding, and the third RBD is in the close down position without mACE2 binding (Figs. 5b and 5d). We observed similar RBD-RBD interaction in all mACE2 complexes

with the spike trimer of BA.1 and BA.2, which is consistent with the similar interaction in Omicron spike trimer-hACE2 complexes. A BA.2-mACE2 complex structure with all three RBDs bound to mACE2 in the open up conformation was also obtained at 4.5 Å resolution upon further particle classification (Supplementary information, Fig. S6e). Local refinement of the RBD-ACE2 region produced a high-quality map of BA.2 RBD-mACE2 and BA.1 RBD-mACE2 at 2.37 Å and 3.01 Å resolution, respectively, which allowed unambiguous model buildings of the RBD-mACE2 complexes (Figs. 5e, 5f, Supplementary information, Figs. S6 and S7). Structure comparison of the BA.2 RBD-mACE2 complex with the BA.1 RBD-mACE2 complex shows a similar overall organization, which also resembles the Omicron RBD-hACE2 complex.

Molecular interactions between mACE2 and Omicron RBDs

Besides the observed structures of BA.2 RBD-mACE2 and BA.1 RBD-mACE2 complexes, the structure of WT RBD-mACE2 complex was modelled for structure comparison to elucidate the significant differences in binding abilities of mACE2 to three spike trimers from SARS-CoV2 WT, Omicron BA.1, and BA.2 strains. By close examination of the three structures, local divergences were found at the RBD-ACE2 interfaces. Despite the existing interactions formed by shared residues on RBDs to mACE2, the mutations on BA.2 form additional interactions with mACE2, including interactions from RBD mutations Q493R, Q498R, and N501Y to mACE2 (Figs. 6a and 6b). In particular, the R493 mutation forms three hydrogen bonds with N31 and Q34, and the side chain of R498 forms one hydrogen bonds with Q42. Notably, the side chain of R493 and R498 of BA.2 RBD form salt bridges with E35 and D38, respectively. Although the additional electrostatic contacts are the major driving force for the interactions between BA.2 RBD and the negatively charged surface of mACE2, the N501Y mutation forms extensive π-π stacking interactions with residues H353 on mACE2, which enhanced the binding between the BA.2 spike trimer and mACE2. The interactions between BA.1 RBD and mACE2 is in a similar way within BA.2 RBD-mACE2 complex (Figs. 6c and 6d), which is consistent with the sequence alignment. Collectively, our results indicate that the three mutations of Q493R, Q498R, and N501Y are essential for mACE2 binding.

Given that ACE2 is highly conserved among the mammals including mouse and human, we aligned the two structures of BA.2 RBD-hACE2 and BA.2 RBD-mACE2 with the root

mean square deviation of 0.482 Å for 670 C_α atoms. Six conserved residues from both mACE2 and hACE2 contribute to the RBD-ACE2 binding, including S19, E35, D38, Y41, Q42, and D355, which form hydrogen bonds or salt bridges with the BA.1 and BA.2 spike trimers (Figs. 7a and 7b). In addition, the side chain of H353 in mACE2 makes extra π-π stacking with Y501 from both BA.1 and BA.2 RBDs. In accordance with our binding data, our structures support that both mACE2 and hACE2 bind to the BA.1 and BA.2 spike trimer with similar affinity.

DISCUSSION

BA.2, a new variant of Omicron, has rapidly spread throughout the world and has become the dominant strain due to its higher infectivity than BA.1. In this study, we first biochemically analyzed the binding affinity of the BA.2 spike trimer to hACE2, which showed around 2-fold higher affinity than that of BA.1 and 11-fold higher affinity than that of the WT strain. The spike-ACE2 interaction is the first step of viral binding to the host receptor, which is critically important for viral entry and subsequent infections. Thus, the higher binding potency of the BA.2 spike trimer is likely contributed to its higher transmission capability. The structure of the BA.2 spike trimer with hACE2 reveals extensive interaction networks in the RBD-hACE2 interface, which is also conserved in the BA.1 spike trimer-hACE2 complex. The network of interaction of the BA.2 spike trimer with hACE2 is more extensive than the WT spike trimer-ACE2 complex, providing a structure basis for the high binding affinity of the BA.2 spike trimer to hACE2. In addition, the RBD of BA.2 is more stable than the BA.1 RBD because of an additional interaction of R403 with D405N in BA.2, which is missing in BA.1 (Fig. 1e). The higher stability of the BA.2 RBD than that of the BA.1 RBD might also contribute to the higher binding affinity of the BA.2 RBD to hACE2 because the high stability of the structure reduces the binding energy cost associated with entropy loss upon binding.

Like the BA.1 strain, BA.2 also harbors many mutations that help its decreased sensitivity to many neutralizing monoclonal antibodies (mAbs). In addition, 4 missense mutations of S371F, T376A, D405N, and R408S in BA.2 RBD but not in BA.1 RBD could also potentially increase the immune evasion of neutralizing antibodies and vaccination, which brings the challenge to effectively subdue the current COVID-19 pandemic.

Despite less severe symptoms in the general population infected with Omicron subvariants, immunocompromised people with underlying diseases are still at high risk of developing severe forms of COVID-19. Antibody therapy could serve as a viable option for these patients either as a preventive treatment or therapeutic. However, several monoclonal antibodies available in clinical practice have shown decreased sensitivity to Omicron BA.1 and BA.2 variants.[28] Thus, broad-spectrum anti-SARS-CoV-2 antibodies, especially with potent activities against Omicron variants are currently in urgent need. Strikingly, we reconfirmed the strong efficacy of our previously discovered antibody, JMB2002, against Omicron BA.2 in both binding assays and pseudovirus neutralization assay, with comparable inhibition potency to Omicron BA.1 strain. Further structural studies of JMB2002 Fab-bound Omicron BA.2 spike trimer enabled us to propose the inhibition mechanism of JMB2002 against Omicron BA.2, similar to the inhibition of Omicron BA.1 by JMB2002. As for Omicron BA.1, structural analysis reveals that the binding of JMB2002 (IgG or Fab) to the BA.2 spike trimer can completely blocks ACE2 binding, thus providing the basis for inhibition of both Omicron BA.1 and BA.2 variants by JMB2002.

In addition, our results also provided a possible origin host for Omicron BA.1 and BA.2. As reported, Omicron evolved independently of all other variants of concerns and its origin is a mystery. Investigation of the origin of Omicron BA.1 and BA.2 is critical for the effective control and prevention of COVID-19 in the human population. Mutation profile analysis suggests that the Omicron variants may have arisen through evolution via the mouse as a host.[4] In this study, our biochemical data confirmed that BA.1 and BA.2 spike trimers are able to bind with high affinity to mouse ACE2 and cat ACE2, while the original WT spike binds well to cat ACE2 but not to mouse ACE2, indicating high susceptibility of mouse and cat to BA.1 and BA.2 infections (Fig.7c). We determined the structures of spike trimers from both BA.1 and BA.2 in complex with mouse ACE2, and our structures elucidated that the three residue mutations Q493R, Q498R, and N501Y are essential for mACE2 binding, suggesting their importance in infections. Intriguingly, mutations on these three residues Q493, Q498, and N501, were detected in the mouse-adapted SARS-CoV-2.[29-31] Surprisingly, the Q498R and Q493R mutations were detected in mouse-adapted SARS-CoV-2 by passage 10 and passage 20, respectively, and have not since been detected in any SARS-CoV-2 variants from other animals.[32] Based on

our data reported here, combined with previous studies, we propose mouse is likely a host for evolution of Omicron variants.

Taken together, our data reveal structural and biochemical insights into the enhanced transmissibility and antibody inhibition of Omicron BA.2 as well as a possible evolutionary pathway for Omicron variants, likely originated from human to cat, then to mouse, then back to human. Although such an evolution pathway is highly speculative, the ability for Omicron variants to infect and spread in mice and possibly other animals could have important implications in the establishment of control strategy in combating SARS-CoV-2 infection.

REFERENCES

1 Dong E, Du H, Gardner L. An interactive web-based dashboard to track COVID-19 in real time. *Lancet Infect Dis* 2020; **20**:533-534.
2 Genomic epidemiology of SARS-CoV-2 with global subsampling. Available from: https://nextstrain.org/ncov/.
3 Yin W, Xu Y, Xu P *et al.* Structures of the Omicron spike trimer with ACE2 and an anti-Omicron antibody. *Science* 2022; **375**:1048-1053.
4 Sun Y, Lin W, Dong W, Xu J. Origin and evolutionary analysis of the SARS-CoV-2 Omicron variant. *J Biosaf Biosecur* 2022; **4**:33-37.
5 Walls AC, Park Y-J, Tortorici MA, Wall A, McGuire AT, Veesler D. Structure, Function, and Antigenicity of the SARS-CoV-2 Spike Glycoprotein. *Cell* 2020; **181**:281-292.e286.
6 Benton DJ, Wrobel AG, Xu P *et al.* Receptor binding and priming of the spike protein of SARS-CoV-2 for membrane fusion. *Nature* 2020; **588**:327-330.
7 Wu CR, Yin WC, Jiang Y, Xu HE. Structure genomics of SARS-CoV-2 and its Omicron variant: drug design templates for COVID-19. *Acta pharmacologica Sinica* 2022:1-13.
8 Lan J, Ge J, Yu J *et al.* Structure of the SARS-CoV-2 spike receptor-binding domain bound to the ACE2 receptor. *Nature* 2020.
9 Shang J, Ye G, Shi K *et al.* Structural basis of receptor recognition by SARS-CoV-2. *Nature* 2020.
10 Yan R, Zhang Y, Li Y, Xia L, Guo Y, Zhou Q. Structural basis for the recognition of SARS-CoV-2 by full-length human ACE2. *Science* 2020; **367**:1444-1448.
11 Wang Q, Zhang Y, Wu L *et al.* Structural and Functional Basis of SARS-CoV-2 Entry by Using Human ACE2. *Cell* 2020; **181**:894-904.e899.
12 Fan X, Cao D, Kong L, Zhang X. Cryo-EM analysis of the post-fusion structure of the SARS-CoV spike glycoprotein. *Nat Commun* 2020; **11**:3618.
13 Cao Y, Su B, Guo X *et al.* Potent Neutralizing Antibodies against SARS-CoV-2 Identified by High-Throughput Single-Cell Sequencing of Convalescent Patients' B Cells. *Cell* 2020; **182**:73-84.e16.
14 Corti D, Purcell LA, Snell G, Veesler D. Tackling COVID-19 with neutralizing monoclonal antibodies. *Cell* 2021; **184**:3086-3108.
15 Li D, Edwards RJ, Manne K *et al.* In vitro and in vivo functions of SARS-CoV-2 infection-enhancing and neutralizing antibodies. *Cell* 2021; **184**:4203-4219.e4232.

16 Collier DA, De Marco A, Ferreira IATM *et al.* Sensitivity of SARS-CoV-2 B.1.1.7 to mRNA vaccine-elicited antibodies. *Nature* 2021; **593**:136-141.
17 Xu J, Xu K, Jung S *et al.* Nanobodies from camelid mice and llamas neutralize SARS-CoV-2 variants. *Nature* 2021; **595**:278-282.
18 Li Q, Zhang M, Liang Z *et al.* Antigenicity comparison of SARS-CoV-2 Omicron sublineages with other variants contained multiple mutations in RBD. *MedComm* 2022; **3**:e130.
19 Cui Z, Liu P, Wang N *et al.* Structural and functional characterizations of infectivity and immune evasion of SARS-CoV-2 Omicron. *Cell* 2022.
20 Han P, Li L, Liu S *et al.* Receptor binding and complex structures of human ACE2 to spike RBD from omicron and delta SARS-CoV-2. *Cell* 2022; **185**:630-640.e610.
21 Suzuki R, Yamasoba D, Kimura I *et al.* Attenuated fusogenicity and pathogenicity of SARS-CoV-2 Omicron variant. *Nature* 2022; **603**:700-705.
22 Gu C, Cao X, Wang Z *et al.* A human antibody of potent efficacy against SARS-CoV-2 in rhesus macaques showed strong blocking activity to B.1.351. *mAbs* 2021; **13**:1930636.
23 Planas D, Saunders N, Maes P *et al.* Considerable escape of SARS-CoV-2 Omicron to antibody neutralization. *Nature* 2021.
24 Liu L, Iketani S, Guo Y *et al.* Striking antibody evasion manifested by the Omicron variant of SARS-CoV-2. *Nature* 2021.
25 Cao Y, Wang J, Jian F *et al.* Omicron escapes the majority of existing SARS-CoV-2 neutralizing antibodies. *Nature* 2021.
26 Yu J, Collier A-rY, Rowe M *et al.* Neutralization of the SARS-CoV-2 Omicron BA.1 and BA.2 Variants. *New England Journal of Medicine* 2022.
27 Wu L, Chen Q, Liu K *et al.* Broad host range of SARS-CoV-2 and the molecular basis for SARS-CoV-2 binding to cat ACE2. *Cell discovery* 2020; **6**:68.
28 Bruel T, Hadjadj J, Maes P *et al.* Serum neutralization of SARS-CoV-2 Omicron sublineages BA.1 and BA.2 in patients receiving monoclonal antibodies. *Nature medicine* 2022.
29 Dinnon KH, 3rd, Leist SR, Schäfer A *et al.* A mouse-adapted model of SARS-CoV-2 to test COVID-19 countermeasures. *Nature* 2020; **586**:560-566.
30 Huang K, Zhang Y, Hui X *et al.* Q493K and Q498H substitutions in Spike promote adaptation of SARS-CoV-2 in mice. *EBioMedicine* 2021; **67**:103381.
31 Leist SR, Dinnon KH, 3rd, Schäfer A *et al.* A Mouse-Adapted SARS-CoV-2 Induces Acute Lung Injury and Mortality in Standard Laboratory Mice. *Cell* 2020; **183**:1070-1085.e1012.
32 Wong LR, Zheng J, Wilhelmsen K *et al.* Eicosanoid signaling blockade protects middle-aged mice from severe COVID-19. *Nature* 2022.

AUTHOR CONTRIBUTIONS

Y.X., C.W. and W.Y. designed the expression constructs, purified the spike complex proteins, screened the cryo-EM conditions, prepared the cryo-EM grids, and participated in figure and manuscript preparation. Y.X. collected cryo-EM images with the help of Q.Y., K.W., Y.X. performed density map calculations, built and refined the models. H.L. participated in figure and manuscript preparation. C.W., M.J. and X.X.W. purified the ACE2 proteins. S-J. D. supervised X.C., C.G., J.L., D.W., X.H. and X.P.W., provided the

JMB2002 antibodies, performed the function assays for JMB2002 antibodies and spike proteins, and participated in manuscript writing; H.E.X. and W.Y. conceived and supervised the project, analyzed the structures, and wrote the manuscript with inputs from all authors.

ACKNOWLEDGMENTS

The cryo-EM data of the Omicron spike protein complexes were collected at the Shanghai Advanced Electron Microscope Center, Shanghai Institute of Material Medica. This work was partially supported by Ministry of Science and Technology (China) grants (2018YFA0507002 to H.E.X.); Shanghai Municipal Science and Technology Major Project (2019SHZDZX02 to H.E.X.); Shanghai Municipal Science and Technology Major Project (H.E.X.); CAS Strategic Priority Research Program (XDB37030103 to H.E.X.), National Natural Science Foundation of China (32130022 to H.E.X.); the Youth Innovation Promotion Association of CAS (2021278 to W.Y.); National Natural Science Foundation of China (32171189 to W.Y.); National Science Fund for Excellent Young Scholars (82122067 to W.Y.); Key tasks of the Lingang Laboratory (LG202103-03-05 to W.Y.); Key tasks of Lingang Laboratory (LG202101- 01-03 to Y. X.); National Natural Science Foundation of China (81902085 to Y. X.); In addition, this work was partially supported by High-level new R&D institute (2019B090904008), and High-level Innovative Research Institute (2021B0909050003) from Department of Science and Technology of Guangdong Province.

Competing interests

H.E.X., W.Y., Y.X., C.W., H.L., M.J., X.X.W., Q.Y and K.W. have declared no competing interest. S-J. D., X.C., C.G., J.L., D.W., X.H. and X.W., are employee of Shanghai Jemincare Pharmaceuticals, and are developing JMB2002 as a potential anti-Omicron therapeutic.

Data Resources

Materials are available from the corresponding authors upon reasonable request. Density maps and structure coordinates have been deposited in the Electron Microscopy Data Bank (EMDB) and the Protein Data Bank (PDB) with accession codes EMD-XXXX and XXXX for; EMD-XXXX and XXXX for; EMD-XXXX and XXXX for;and EMD-XXXX and XXXX for. Source data are provided with this paper.

Figure legends

Fig 1. **SARS-CoV-2 Omicron BA.2 spike protein with higher affinity to human ACE2.**

a. The infectious frequency of SARS-CoV-2 Delta, Omicron BA.1, and Omicron BA.2 strains since January 2022 to April 2022.

b. Binding of Omicron BA.2 spike protein to human ACE2 determined by BLI. K_D values were determined with Octet Data Analysis HT 11.0 software using a 1:1 global fit model.

c. Relative potency of WT, BA.1, and BA.2. K_D values were determined by BLI method.

d-e. Cryo-EM density of the hACE2-Omicron BA.2 spike trimer complexes with hACE2 and BA.2 spike in 3:3 molar ratio (d) or in 2:3 molar ratio (e).

f. The locations of Omicron BA.2 mutations on the Spike trimer. Spike trimer is shown in surface. The shared mutations between BA.1 and BA.2 are colored in green and the BA.2 its own mutations are colored in red.

g. The locations of 16 Omicron BA.2 mutations on the RBD. RBD is shown in surface. The shared mutations between BA.1 and BA.2 are colored in green and the BA.2 its own mutations are colored in red, including S375F, T376A, D405N, R408S, and N440K.

Fig 2. **Structural analysis of Omicron BA.2 RBD and hACE2.**

a. Cryo-EM density of Omicron BA.2 RBD-hACE2 bound region. Residues are shown in sticks with the correspondent cryo-EM density represented in mesh. hACE2 is colored in coral. The Omicron BA.2 RBD is colored in purple.

b. Detailed analysis of interactions between Omicron BA.2 RBD and hACE2.

c. Comparison of Omicron BA.2 RBD-hACE2 and WT RBD-hACE2 interfaces. Up panels, Omicron BA.2 RBD-hACE2 with hydrogen bonds and salt bridges interactions. Down panels, WT RBD-hACE2 with hydrogen bonds and salt bridges interactions. WT RBD is colored in pink, Omicron BA.2 RBD is colored in purple, BA.2 RBD bound hACE2 is colored in coral, and WT RBD bound hACE2 is colored in orange. Interactions of hydrogen bonds and salt bridges are in dotted lines.

d. Thermal stability shift analysis of the Omicron BA.2, Omicron BA.1, and WT spike trimer.

e. The mutation-induced conformation changes of Omicron BA.2 RBD comparing with WT RBD.

FIG. 3. Inhibition of ACE2 binding to the Omicron BA.2 spike trimer by an anti-Omicron antibody JMB2002.

a. Binding of JMB2002 Fab and IgG to the Omicron and WT spike trimer.

b. Inhibition of the pseudovirus of Omicron BA.2 by JMB2002.

c. Cryo-EM density map of the Fab-bound Omicron BA.2 spike trimer shown as front and top views.

d. Top view of Fab-bound Omicron BA.2 spike trimer complex model with Fab and nanobody hidden.

e. Superposition of the ACE2-bound and Fab-bound Omicron BA.2 spike trimer showing that Fab binding to RBD inhibits ACE2 binding

FIG. 4. Characterization of the binding affinity between mouse ACE2 and Omicron spike trimer proteins

(**a-c**) Binding of Omicron BA.2 (a), Omicron BA.1(b) and WT (c) spike trimers to mouse ACE2 as determined by BLI.

d. Amino acid alignment of the 16 key residues in hACE2 with 4 ACE2 orthologs from mouse, cat, rat, and dog.

e. The K_D values of tested pairs in this study as determined by BLI.

f. Superposition of the structures of human ACE2 bound Omicron BA.2 spike trimer and the cat ACE2 bound original spike trimer, showing the detained interactions.

(**g-h**) The binding modes of dog (g) and rat (h) ACE2s with the BA.2 RBD, were generated based the complex structure of human ACE2 bound Omicron BA.2 spike trimer. The differentiated residues among ACE2 proteins that are responsible for the interactions with SARS-CoV-2 spike protein are showed with detained interactions.

Fig.5. Cryo-EM structure of the Omicron BA.2 and BA.1 spike timers in complex mouse ACE2 protein

(**a-b**) Cryo-EM maps of the Omicron BA.2 spike protein-mACE2 complex with one RBD in “up” conformation at 3.2-Å resolution (a), and mACE2 complex with two RBD in “up” conformation at 3.3-Å resolution (b), respectively. The three protomers are colored in purple,red and green, the density for bound ACE2 is colored in coral.

(**c-d**) Cryo-EM maps of the Omicron BA.1 spike protein-mACE2 complex with one RBD in “up” conformation at 3.2-Å resolution (c), and mACE2 complex with two RBD in “up” conformation at 3.3-Å resolution (d), respectively. The three protomers are colored in purple,red and green, the density for bound ACE2 is colored in coral.

(**e-f**) Representative densities and atomic models of the interaction interfaces of Omicron BA.2 spike protein-mACE2 complex (e) and Omicron BA.1 spike protein-mACE2 complex (f), showing the detained interactions in sticks.

Figure 6. Structural analysis of mACE2 and RBD.

a. Overall structure of BA.2-RBD and mACE2.

b. Details of the binding between BA.2-RBD and mACE2. The binding between the receptor binding motif of BA.2-RBD and mACE2 consists mainly of two interaction fields, marked in a red and a blue box, respectively. Residues involved in the interaction are shown as sticks and labeled. Hydrogen bonds are shown as dashed black lines.

(**c and d**) Overall structure of BA.1-RBD and mACE2, with detailed hydrogen bond or salt bridge interactions in BA.1-RBD and ACE2 interfaces with the same view as in (a and b).

(**e and f**) Overall structure of the superposition of BA.2 RBD ACE2 complex with SARS-CoV-2 WT-RBD (PDB: 6LZG), with detailed hydrogen bond or salt bridge interactions in WT-RBD and ACE2 interfaces with the same view as in (a and b).

Figure 7. Comparison of the binding mode to BA.2-RBD between mACE2 and hACE2.

a. Detailed structure of the superposition of the BA.2-RBD and mACE2 complex with the BA.2-RBD and hACE2 complex, with hydrogen bond or salt bridge interactions shown as dashed lines. Hydrogen bond or salt bridge interactions in hACE2-RBD and mACE2-RBD are shown as red and black dashed lines, respectively.

b. Residues involved in the interaction of BA.2-RBD with hACE2 or mACE2 are listed and connected by lines. Red dashed lines indicate one H-bond or salt bridge and red solid lines indicate two H-bonds or salt bridges, whereas the cyan solid line represents a π-π stacking interaction between the residues.

c. A brief summary of the infection patterns of BA.1, BA.2 and WT in human, mouse and cat.

Figure 1

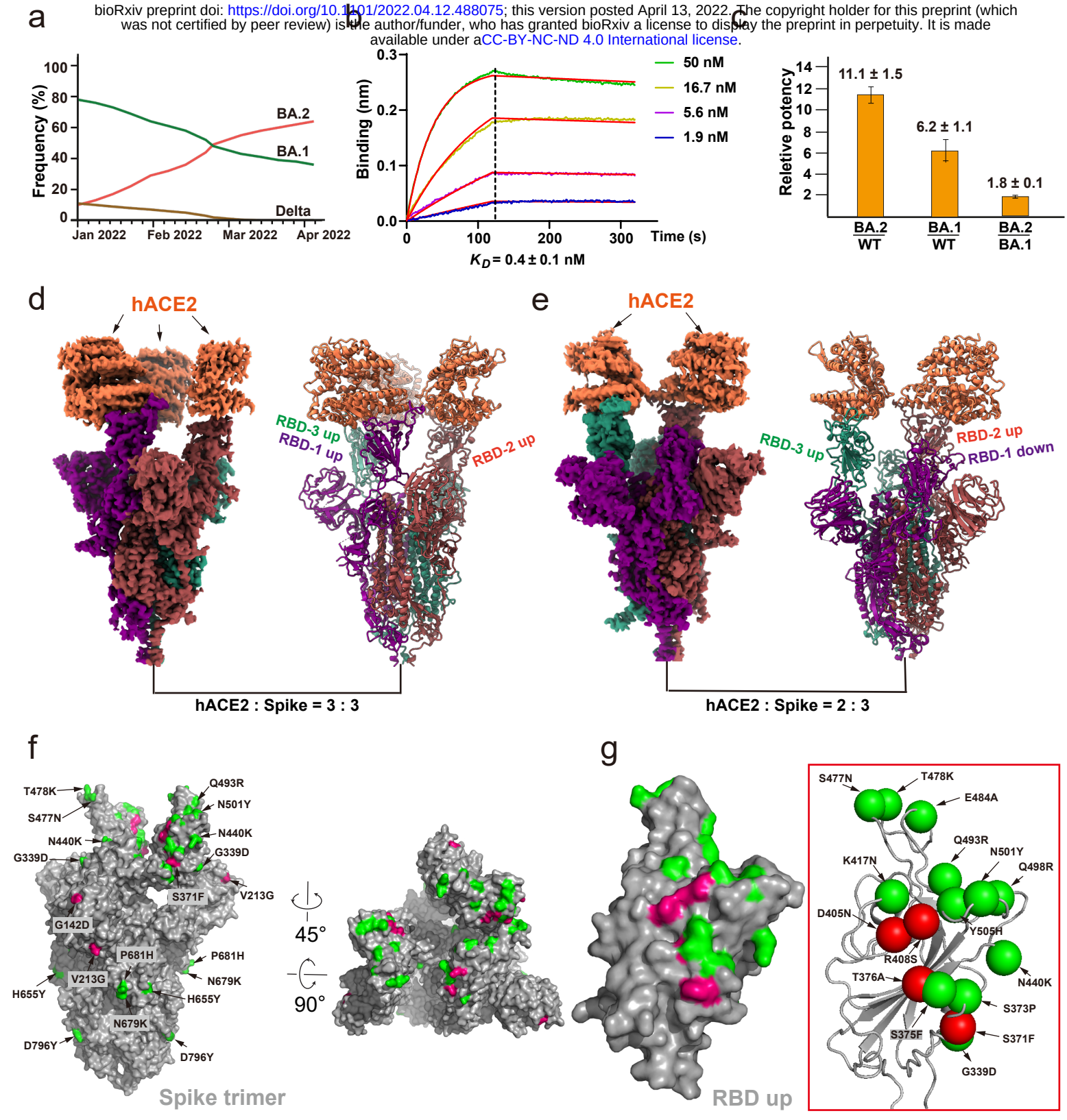

Figure 2

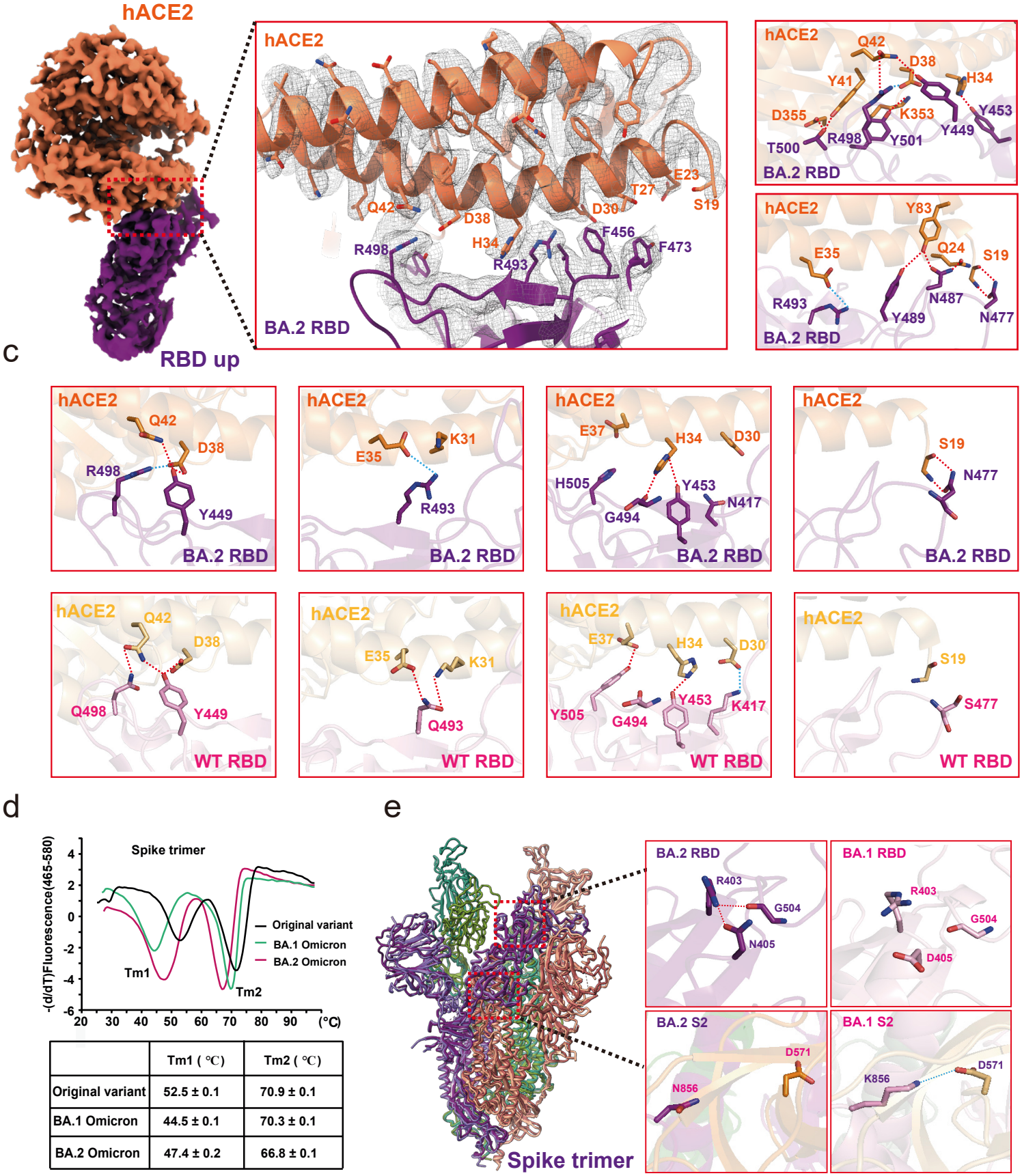

	Tm1 (℃)	Tm2 (℃)
Original variant	52.5 ± 0.1	70.9 ± 0.1
BA.1 Omicron	44.5 ± 0.1	70.3 ± 0.1
BA.2 Omicron	47.4 ± 0.2	66.8 ± 0.1

Figure 3

a

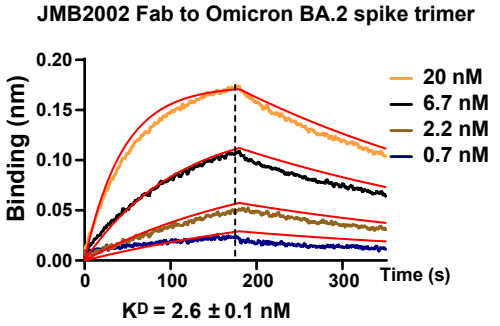

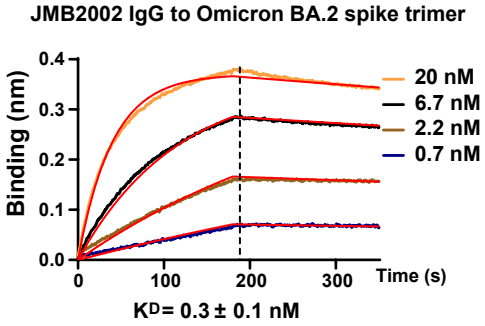

b

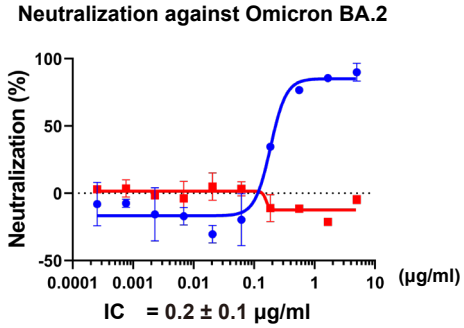

c

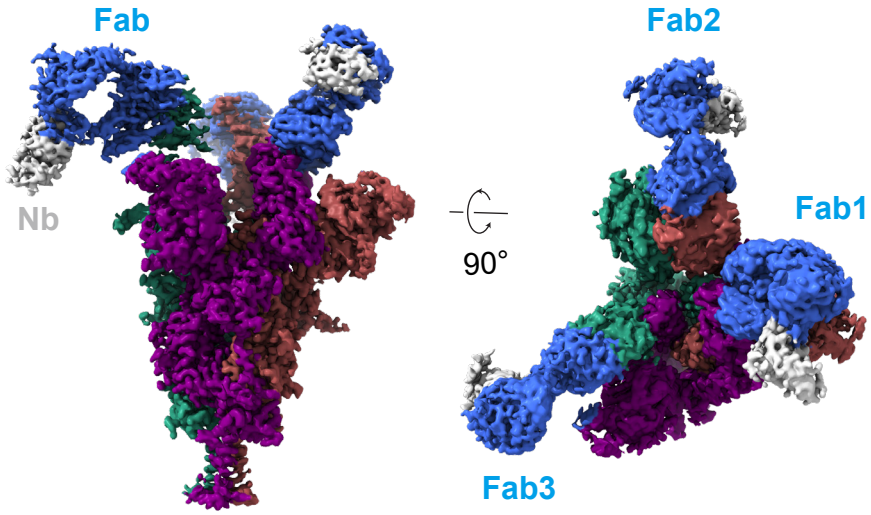

d

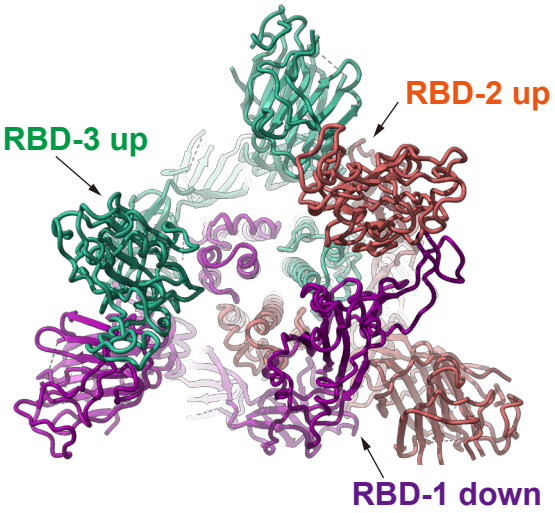

e

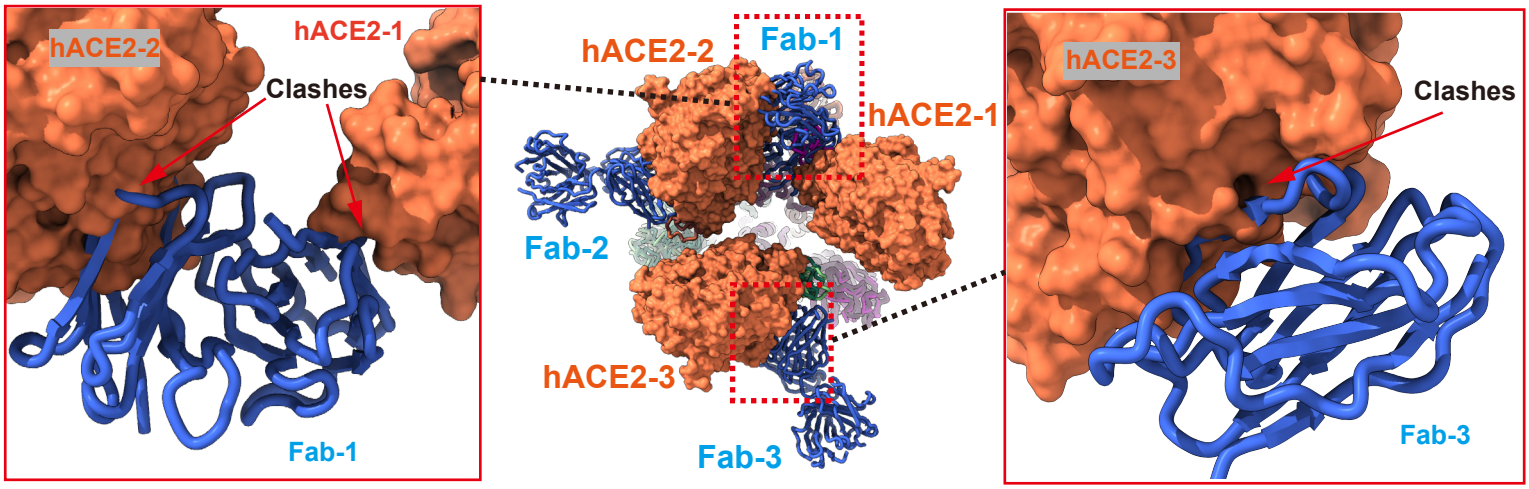

Figure 4

a

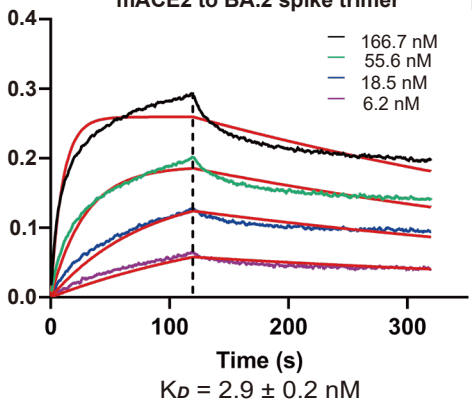

KD = 2.9 ± 0.2 nM

b

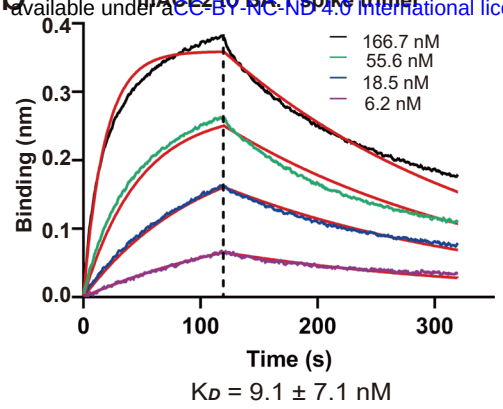

KD = 9.1 ± 7.1 nM

c

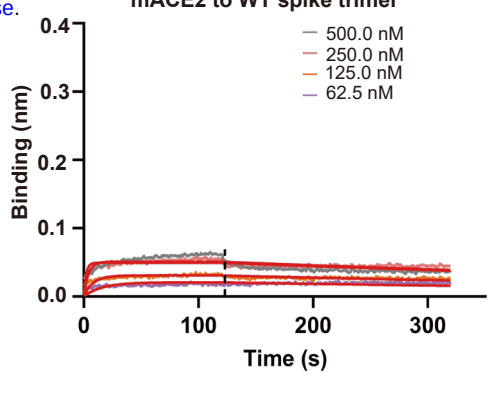

d

Species (ACE2)	KD value to Spike ECD Trimer (nM)		
	BA.2	BA.1	WT
Human	3.2 ± 0.7	6.4 ± 1.0	15.0 ± 0.6
Mouse	2.9 ± 0.2	9.1 ± 7.1	>200.0
Cat	16.6	4.4	10.2
Rat	>500.0	>500.0	>500.0
Dog	>500.0	>500.0	>500.0

e

	19	24	27	28	30	31	34	35	38	41	42	45	82	83	353	355
Human	S	Q	T	F	D	K	H	E	D	Y	Q	L	M	Y	K	D
Mouse	S	N	T	F	N	N	Q	E	D	Y	Q	L	S	F	H	D
Cat	S	L	T	F	E	K	H	E	E	Y	Q	L	T	Y	K	D
Rat	S	K	S	F	N	K	Q	E	D	Y	Q	L	N	F	H	D
Dog	S	L	T	F	E	K	Y	E	E	Y	Q	L	T	Y	K	D

f

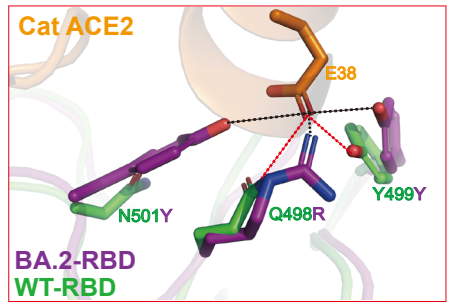

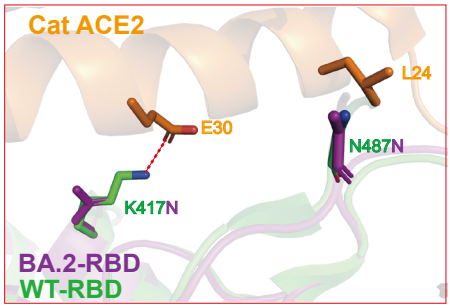

g

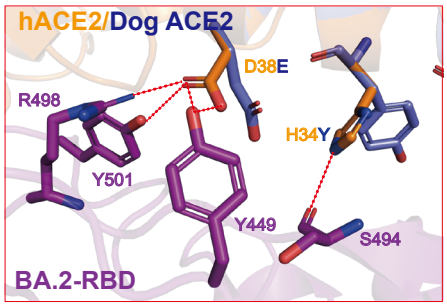

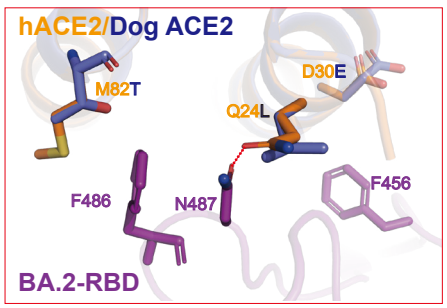

h

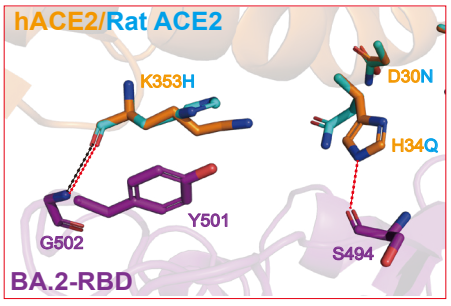

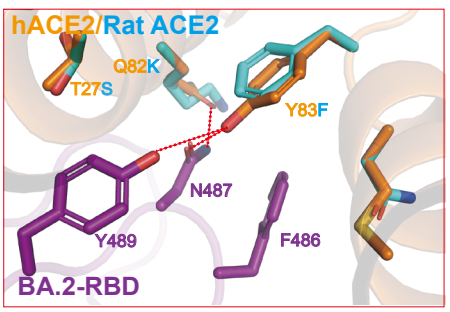

Figure 5

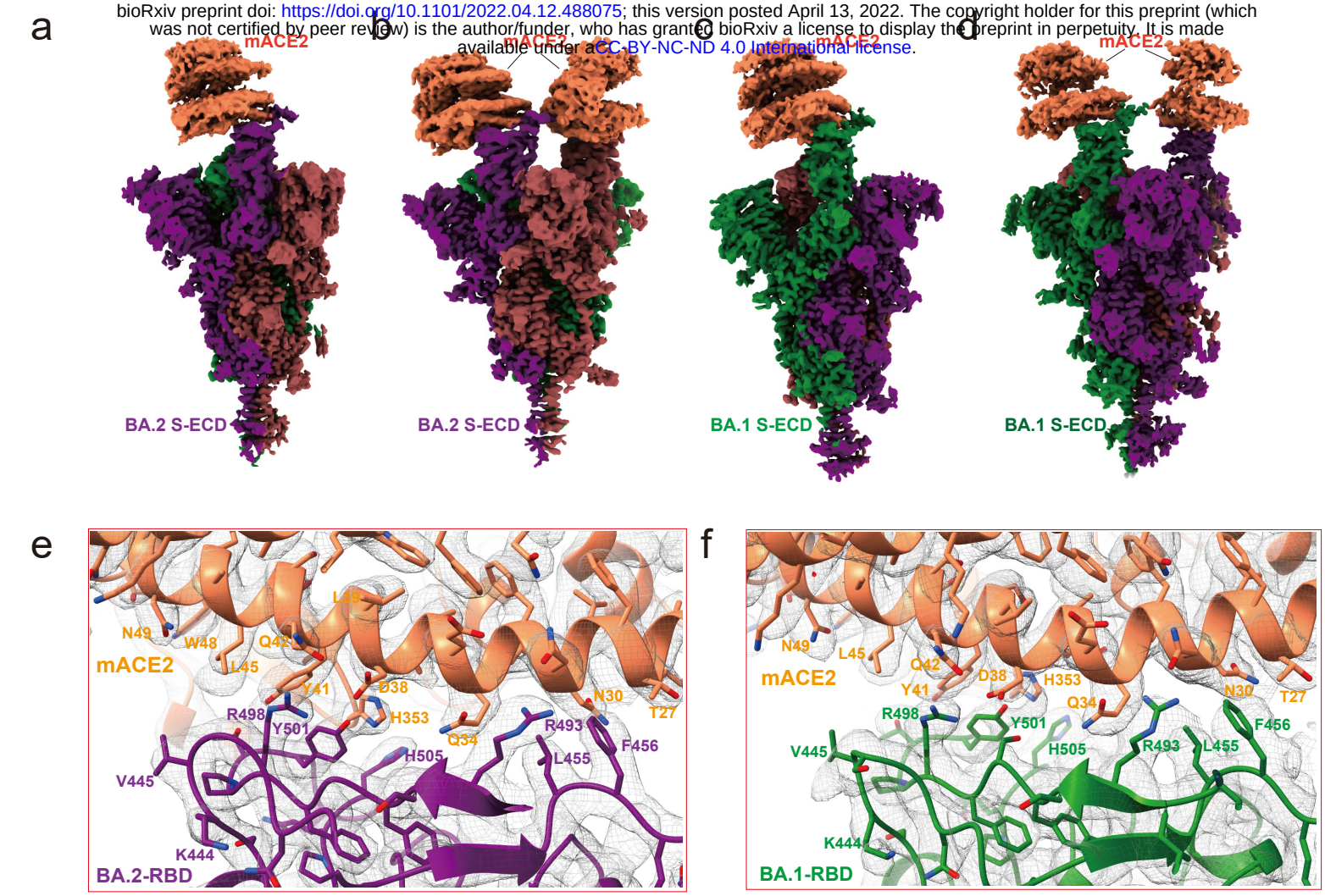

Figure 6

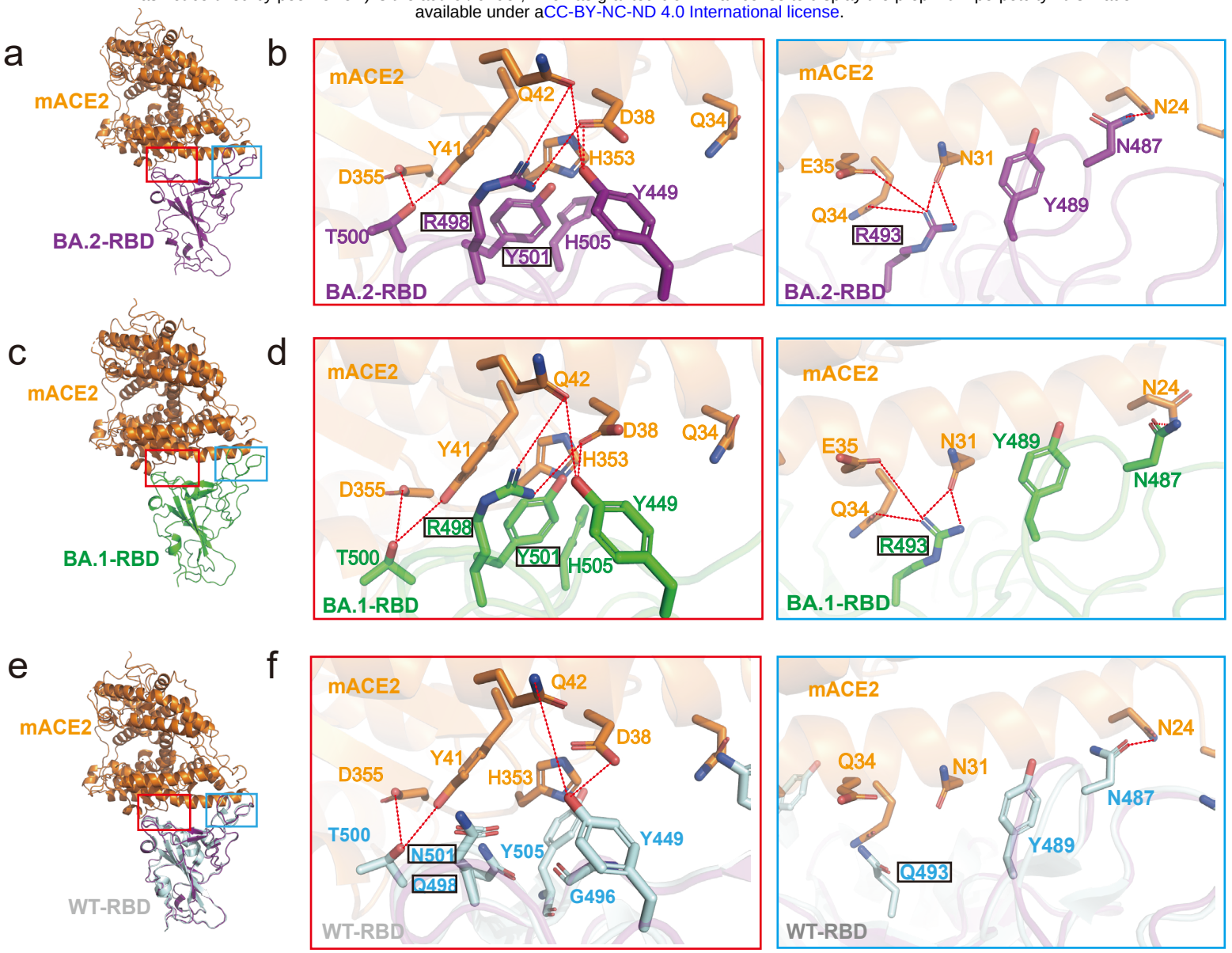

Figure 7

a

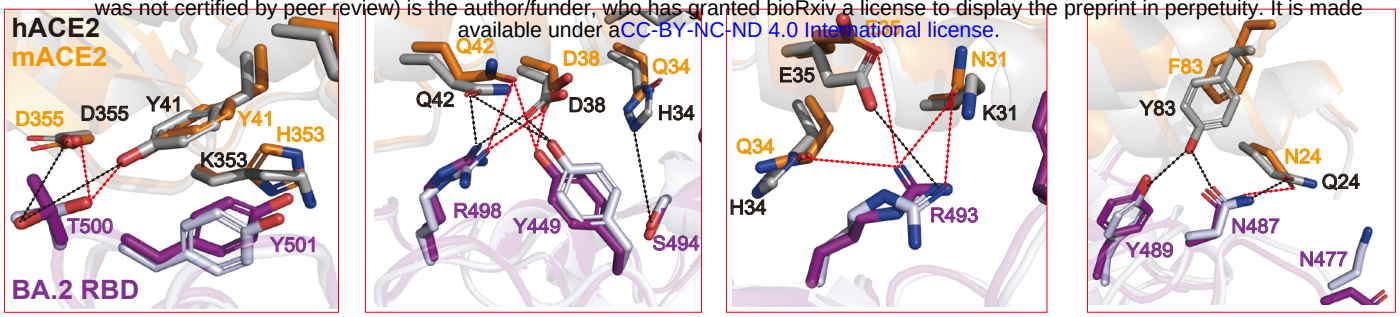

b

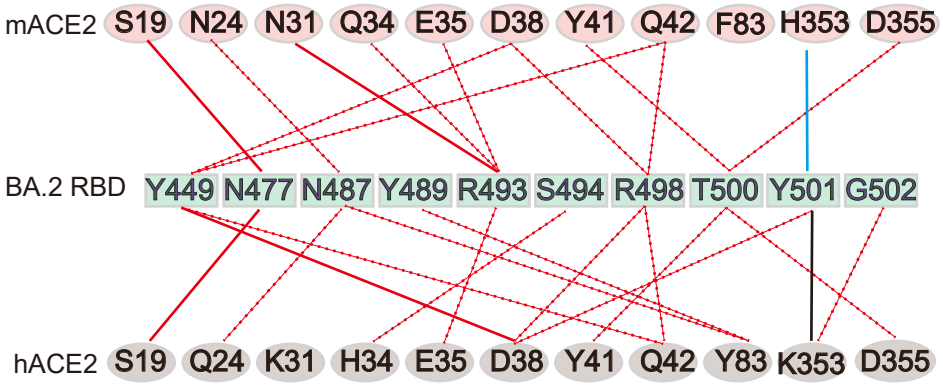

c